International Journal of Engineering & Technology, 7 (3.17) (2018) 254-259

International Journal of Engineering & Technology

Website: www.sciencepubco.com/index.php/IJET

Research paper

Surface Roughness Effects on Turbulent Boundary Layer Structure of NACA 0026 Airfoil

A. A. Abbas[1] , W. A. W. Ghopa[1] , S. Mat[2] , K.-S. Choi[3] , M. F. Abdullah[1] , Z. Harun[1,*]

[1)]Centre for Integrated Design for Advanced Mechanical System (PRISMA),
Faculty of Engineering and Built Environment
Universiti Kebangsaan Malaysia
43600 Bangi, Malaysia
[2)]Solar Energy Research Institute (SERI)
Universiti Kebangsaan Malaysia
43600 Bangi, Malaysia
[3)]Faculty of Engineering
University of Nottingham
Nottingham NG72RD, UK
**Corresponding author E-mail:zambri@ukm.edu.my*

Abstract

This research addresses the understanding of initial experimental results from an ongoing investigation of the riblets effects on the behaviour of turbulent boundary layer over a rough surface applied onto the surface of NACA 0026 airfoil in a herringbone pattern, via a low-speed wind tunnel. Riblets arranged in directionally converging-diverging pattern, approximately 7.5% in chord percentage, riblets are attached and flushed to the airfoil surface. Riblets are yawed at $\alpha = 0o$ and $\pm 10o$ with dimensions of height, $h = 1$ mm and spacing, $s = 2$ mm. The airfoil with external geometry of 500 mm span, 600 mm chord, and 156 mm maximum thickness has been built using mostly woods and aluminium. The application of riblets significantly affects boundary layer thickness. At Reynolds number $Re\tau \approx 200$ and freestream velocity $U\infty \approx 5$ m/s. We observe that riblets cause boundary layer and turbulence intensities profiles to change drastically. Upon exposure to riblets, both boundary layer and turbulence intensities profiles on NACA 0026 airfoil follow closely with that of favourable pressure gradient (FPG) flows. Without riblets, the flow has a very small layer of the logarithmic region and high wake (in the velocity profile) and highly energized inner region (in the intensities profiles). Without riblets, the inner region ($z+ = 15$) contains energised $\lambda x+ = 1000$ features as well as very long features measuring 20δ, typically not observed in internal flows. The energy spectra analysis reveals that riblets of any type break these 20δ features in the near-wall to break down into smaller features. This study might shed some lights into research focusing on controlling flow behaviours using surface roughness.

Keywords: *Turbulent boundary layer; Riblets; Converging and diverging; Large-scale features; Airfoil.*

1. Introduction

In the third phase of the emission trading session, the European Commission Emission Trading System (ETS) has set the carbon pollutions to be 21% lower by 2020 in comparison with 2005. This has to be done because of the concerns over the global warming phenomenon, emission and rising fuel costs in the last decades. Finding techniques to control turbulent flow over the surface is an essential method to reduce skin friction, therefore fuel consumptions and emissions. Several techniques have been discovered from nature e.g. animal skin features and movements which are greatly beneficial to reduce skin frictions [3, 4, 7, 9, 36]. One example is mimicking the scale arrangement that of the sharks, this is called the *riblets.* When applied properly with fluid dynamics knowledge, riblets can reduce fuel consumptions due to the reduced skin friction. Riblets application could effectively control turbulent boundary layer and can further be extended in different applications, for instance, the aircraft, windmill blades, pipelines, racing cars, rowing shells, missiles, windsurfers, luge sledges, high-speed train, ship and athletic swimsuits [27, 28]. A technique inspired by the humpback whale's flipper (tubercles) clarified by [1] this technique later applied in different types of airfoil lead to delayed separation event and improve the performance of aircraft. [26] stated that the triangular shape of riblets has the ability to reduce the drag. Also, the smallest resistance of fluid occurs when $h \geq 0.6s$, where h refer to the height and s is the spanwise spacing tip-to-tip (TPT) of a riblet. An investigation by [3, 11] showed the interest from controlling the riblets surface parameters (h and s) work to reduce drag up to 7 – 10 % compared with a smooth surface for both experimentally and direct numerical simulation (DNS) studies. Further investigation by [4] showed that riblets design with relationship $h = 0.5s$ produces a best drag-reducing performance. This study also revealed that the negative drag reduction occurs when the height of riblets approaches $h > 0.6s$.

Furthermore, [37] reported that the tip angle α_t of riblets should not exceed $\alpha_t > 45^o$. Otherwise, it increases friction velocity causing reduced surface roughness performance. Recently [12] showed that the relation between friction velocity and varies tip angle (30^o, 45^o and 60^o is a positive relationship where the shear stress increase with the increase the value of tip angle, while the behavior of boundary layer thickness controlled by the yaw angle α and the arrangement of the surface (converging-diverging). [31]

Copyright © 2018 Authors. This is an open access article distributed under the Creative Commons Attribution License, which permits unrestricted use, distribution, and reproduction in any medium, provided the original work is properly cited.

showed that at different aspect ratio h/s = 1 and h/s = 2 of converging riblets at α = 30º, symmetrical small-scale structures were generated near to the wall region similar to mushroom shape. However, large-scale structures were energized when the structure breakdown at downstream of the riblets. A most recent finding by [14] showed that the herringbone surface with converging-diverging pattern with aspect ratio h/s = 0.5 and yaw angle ±10º, applied onto the surface of a symmetrical airfoil NACA 0026 has the ability to control and modify the turbulent boundary layer thickness, the converging and diverging riblets, cause pronounced outer peaks in the turbulence intensities profiles. Most importantly, flows past converging and diverging pattern experience 30% skin friction reductions. The aim of this paper is to extend the previous experiment by [14]. The directional, diverging and converging riblets pattern applied onto the surface of NACA 0026 airfoil are studied by considering the analysis of turbulent boundary layer profile, turbulence intensity and energy spectra, to understand surface roughness effects over turbulence boundary layer structure.

2. Methodology

The methods are divided into four parts. The first deals with the flow facilities used and the details of the flow in the wind tunnel. The 2nd and 3rd parts provide the preparation steps of the directional, converging-diverging riblets pattern and the key points of the NACA 0026 airfoil with the expected points of boundary layer behaviour over the airfoil respectively. The last involves the explanation of experimental set-up and data acquisition devices used; all these are provided as follows.

2.1 Wind Tunnel Facilities

The experiments were performed in an open-circuit blow-down type, Pangkor low-speed wind tunnel (PLSWT) located at the Beach and Water Engineering Laboratory of Faculty of Engineering and Built Environment, Universiti Kebangsaan Malaysia (UKM). The wind tunnel has a two-dimensional contraction nozzle with area ratio 2.4:1, followed by test section with cross-sectional area 1.2 m × 0.5 m (width × height) and 3 m total length. Fully automated wind tunnel with two-dimensional traverse system which is located at 1.7 m downstream to the inlet of the test section [20]. At free stream velocity U_∞ in the test section of 22 m/s, its free stream turbulence intensity is approximately 0.5% [20]. At sufficiently high wind tunnel Reynolds number, based on the hydraulic diameter $D_H = 2ab/(a+b)$ [38] where a = height and b = width of the test section and centerline velocity at this U_∞, the Reynolds number is Re ≈ 1 × 10^6, at atmospheric condition produced by 30 ºC. The test section is the appropriate size to perform experiments in a zero-pressure gradient. This wind tunnel was previously used by [30] and for further details, see [20] Figure 1 shows the general arrangements of the wind tunnel.

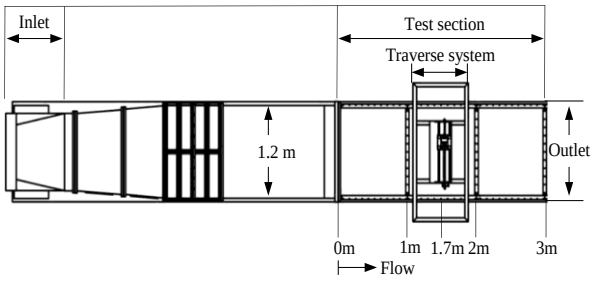


Fig. 1: Schematic diagram of wind-tunnel geometry (Top View)

2.2 Herringbone Surface (Riblets) Fabrication Techniques

The specific dimensions of surface roughness used in this study are shown in Figure 2, where high-precision computer numerical control (CNC) machine with a 60º tool bit was used to carve V-grooves onto an aluminium plate [15]. The mould dimension (500 mm width × 200 mm length) was chosen so that enough space is available to get different size of silicone samples and potentially different arrangement. Riblets grooves are yawed at α = 0º with spanwise spacing and height are s = 2 mm and h = 1 mm respectively, to achieve an aspect ratio of an h/s = 0.5 [4, 37]. Silicone rubber has been used as the primary material for riblets. The replication method was used in order to duplicate the pattern of surface roughness mould in different shapes, dimensions and the features of riblets [5, 6]. Silicone and hardener mix of intended strength and brittleness properties was mixed and then poured evenly onto the aluminium mould after vacuuming process to eject air bubbles, see [14] for further details. The silicone rubber layer was cut by stainless steel utility knife at α = 0º, ±10º for both convergent and divergent riblets. This is the same angle used by [14, 33] and smaller than [23, 35] α = 45º,30º respectively. These samples were arranged such that to obtain the converging-diverging riblets pattern arrangement; the length was 45 mm and width was 50 mm of each diverging and converging, resulting in a repeating spanwise wavelength Λ = 100 mm. Hence, two strips of directional, diverging region and one strip of the converging region, placed at x/c ≈ 23.33 % in chord percentage of the NACA 0026 airfoil. Note that the dimensions of riblets (s and h) have been chosen to be smaller than the streamwise structure length, where the streamwise structure lengths λ equal to $3\delta \approx 34.8$ mm > s = 2 mm and sufficient length to be longer than the boundary layer structure length λ equal to $3\delta \approx 34.8$ mm < 45 mm.

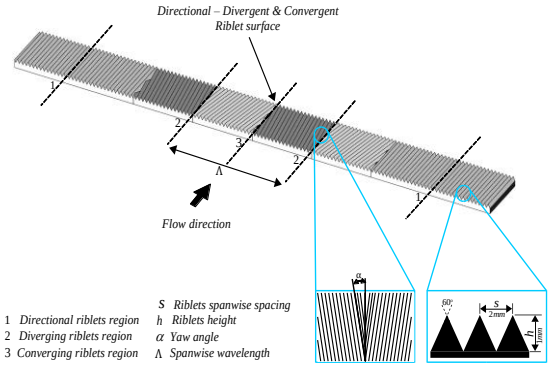


Fig. 2: Schematic diagram showing the key dimensions of herringbone surface type – riblets (directional – diverging and converging pattern) with the details for the cross-sectional area of the riblets strips

2.3 Airfoil Model

Prior to National Aeronautics and Space Administration (NASA), the National Advisory Committee for Aeronautics (NACA) was then the committee to undertake, promote, and institutionalize aeronautical research. NACA standardized the shapes of airfoil used in aircraft wings, the shape of NACA airfoils is described using a series of digits following the word NACA. The design of an airfoil requires expertise in fundamentals of aerodynamics; it then needs to be verified by testing in a wind tunnel. A symmetrical airfoil inspired from a dolphin flipper fin [8] and mostly used by the different application, for instance, light aircraft, tails (vertical & horizontal stabilizer), supersonic jets, helicopter blades, shrouds, missile/rocket fins and wind turbine blade. Hence, DesignFOIL software is used to design and generate the NACA 0026 airfoil. The airfoil design was tested in a 2D virtual wind tunnel, this to understand the pressure distribution and to calculate the estimated coefficient of pressure Cp (refer to

Figure 3). The turbulence level of NACA 0026 starts at 194.7 mm away from leading edge, i.e. $x/c \approx 32.45$ % in chord percentage, where x is the distance from the leading edge, c is the chord length. The airfoil had previously been verified by previous work of [10, 14, 15]. The airfoil has been fabricated using mostly wooden structure, plywood surface, stainless steel support [14, 15]. The chord, c is 600 mm, and the span sp is 500 mm. The thickness, t is 156 mm. The chord line falls on the mean camber line making it a symmetrical airfoil. The span of the airfoil matches the height of the wind tunnel, so when the airfoil is arranged vertical, two-dimensionality issues are greatly minimized. The airfoil was installed by passing a 16 mm diameter stand, made from stainless, through the base of the test section to ensure a rigid support during the experiment. The riblets were applied, flushed on one side of the airfoil at 140 mm from the leading edge, $x/c \approx 23.33\%$ in chord percentage, refers to the black strip in Figure 4. The length of the riblet surface is 45 mm in the streamwise direction. The riblets surfaces were applied between the laminar and transition region, where the transition starts at 28.33% and the turbulence start at $x/c \approx 32.45\%$ in chord percentage [14] of the airfoil surface because of the needs of a sufficient length. The application of riblets cause the boundary layer to develop and grow earlier (than a smooth surface), this leads to the breakdown of boundary layer structure of the laminar flow to turbulence towards the rest of the airfoil until the trailing edge [31].

The NACA 0026 airfoil produces both a favourable pressure gradient (FPG) and adverse pressure gradient (APG) due to the characteristic shape. Figure 3 shows the details of the favourable – adverse pressure distribution pattern of the flow over the smooth surface of the NACA 0026 airfoil at $\alpha_{AoA} = 0^o$, generated via a virtual wind tunnel.

In Figure 3, at the stagnation point ($x/c = 0$), $Cp = 1$, this is an APG environment. Cp drastically drops, the flow experiences FPG after passing the leading edge at $x/c \approx 3\%$. APG regions continues until $x/c \approx 86$ %. The APG region starts again at $x/c \approx 88$ % until the trailing edge. Hence, adequate locations of measurement could be performed [14]. The airfoil Reynolds number ($Re_c = \rho U_\infty l/\mu$) based on the chord length is $Re_c \approx 187000$. Figure 4 provides the location of the laminar, transition and turbulent region, as well as the measurement points, were carried out for both smooth and riblets.

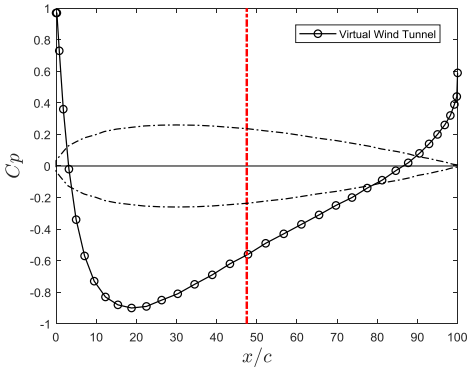


Fig. 3: Pressure coefficient of the smooth surface over NACA 0026 at $\alpha_{AoA} = 0^o$ tested in a virtual wind tunnel generated from DesignFOIL, dashed-dot red vertical lines indicate $Cp \approx -0.55$ at $x/c = 47.5\%$ location of the measurements point in percentage of chord and the dashed-dot black curved lines indicate the shape of the NACA 0026 airfoil

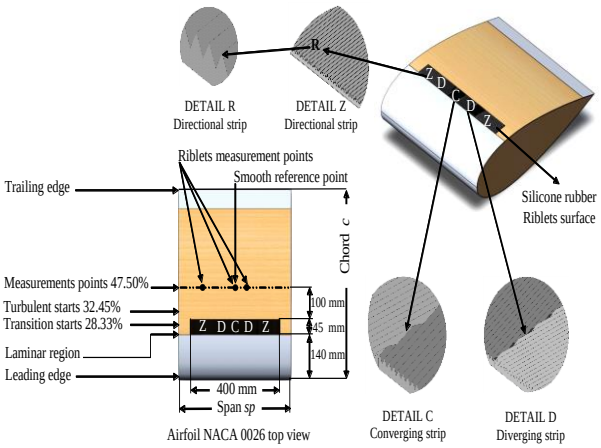


Fig.4: Schematic diagram of a NACA 0026 airfoil showing the dimensions and application of riblet in black strip, the location of transition, the start of turbulent, and the measurements points for both smooth and riblet surfaces boundary layer in chord percentage

2.4 Experimental Set-Up

For the existing experiments, wind tunnel operates at a free stream velocity of $U\infty \approx 5$ m/s. Measurements were carried out with a handmade single hot-wire probe *(Dantec 55P05)* – boundary layer type [14, 29] performed at constant temperature using Dantec's multi-channel CTA system model 54N80 with an overheat ratio of 1 - 1.5. Wollaston wire produced by Sigmund Cohn Corp. with a platinum core diameter of 5 microns (μm) were soldered to the tips of the hot-wire prong and then etched [17]. To address spatial resolution issues appropriately, sensor lengths were etched to approximately 1 - 1.5 mm.

Previous studies [2, 24] reported that the length-to-diameter ratio *(l/d)* of hot-wire sensor should exceed 200 to minimize attenuations due to end conduction effect. The hot-wire data is collected using National Instruments (NI) 9215 module while data from all other sensors such as temperature, static pressure (pitot-tube), atmospheric pressure, room humidity and dew point were collected using Comet, model H7331 [20]. This system allows measurement performed at very high frequency 20 kHz. It is important that high frequency is employed so that turbulence characteristics could be analyzed properly [25]. The hot-wire calibration was performed in-situ.

In this experiment, the angle of attack αAoA have been avoided, this gives a clear understanding of the riblets effects on the NACA 0026 turbulent boundary layer structure at $\alpha AoA = 0$o. The airfoil NACA 0026 (the leading edge) were aligned in a streamwise direction at 1320 mm or at $x/l \approx 44$ % in test section length percentage, where l is the test section length. All the measurements were made at the same streamwise distance from the leading edge $x/c \approx 47.50$ % in chord percentage; different to the previous experiment by [14], where the measurement points were made at $x/c \approx 33$ %, $x/c \approx 44\%$ for both smooth and riblets respectively. The wall-normal measuring points are spaced logarithmically and controlled by an automated two-dimensional traverse system [14, 15] moving in a spanwise direction. These measurements are made at different spanwise locations on the airfoil surface as indicated in Figure 4.

3. Results

3.1 Experimental Parameters

Table 1 consists of the boundary layer parameters for both the smooth-wall and herringbone surface – type riblets. The abbreviations C is for converging, D is for diverging at yaw angle

α = ±10o (for both *C*, *D*) and *Z* is for directional riblets with yaw angle α = 0o and *S* for a smooth surface, *x/c* is the measurements points location in percentage to the chord *c*. $U\infty$ is the free stream velocity, $h+$ is viscous-scaled riblet height, and $s+$ is viscous-scaled riblet spacing, where $h+ = hU\tau/\nu$ and $s+ = sU\tau/\nu$. The boundary layer thickness defines as δ, skin friction velocity Uτ, friction Kármán number Reτ and Cf are the skin frictions.

The two-dimensional traverse system used to position the hot-wire sensor, the Pitot tube, in the centre of the test section of the wind tunnel (free-stream). Two calibrations were performed in-situ using the Pitot; this could overcome the error due to lengthy measurements caused by the change of atmospheric condition. The pre-calibration were carried out before the boundary layer measurements. Temperatures, along with the atmospheric pressure and room humidity were recorded during the pre-calibration. Another calibration process at the end of the experiment, the post-calibration, was also performed. The calibration curves were compared and, if necessary, temperature compensations might have to be implemented. Note that the calibration points are 10 points with the velocity incrementally from zero to slightly above freestream velocity (≈ 200% of U∞).

In each boundary layer measurement, the hot-wire sensor traverses 50 logarithmically spaced wall-normal positions starting at approximately 0.125 mm up to 50 mm. All measurements performed at a frequency of 20 kHz for 180 seconds. The distance of the protruded traverse system's rod to the hot-wire sensor exceeds 12D, where Dt is the traverse rod diameter. Hence the sensor is placed at 120 mm away from the rod. This way, sufficient areas were provided for the boundary layer to develop without obstructions and to overcome the effect of traverse rod to the hot-wire sensor while measurements take plac

Table 1 : Experimental parameters for smooth and rough surfaces, $l^+ = lU\tau/\nu \approx 25 - 35$ for all

Exp Code		Location *x/c* %	U_∞ (m/s)	h^+	s^+	δ (m)	$U\tau$ (m/s)	$Re\tau$	$C_f = 2(U\tau/U_\infty)^2$
C	Converging	47.50	4.9347	17.31	34.63	0.01270	0.275	220	0.0062
D	Diverging	47.50	5.3677	19.42	38.84	0.01132	0.309	220	0.0066
Z	Zero degree /Directional	47.50	5.4682	20.09	40.19	0.01094	0.319	220	0.0068
S	Smooth	47.50	5.5616	-	-	0.01160	0.270	195	0.0047

3.2 Velocities and Turbulence Intensities Profiles

Figure 5 (a) shows the boundary layer velocity profiles over the smooth surface and herringbone surface (directional, converging and diverging) region of the riblets pattern. We use the Clauser method to obtain skin-friction velocity over the rough and smooth surfaces. The vertical axis represents velocity; the overbar indicates mean value, therefore, Ū represents local mean velocity. The vertical axis of the boundary layer is made non-dimensional by the friction velocity U_τ obtained from the Clauser chart method, the lower abscissae is the wall normal coordinate scaled with inner variables U_τ/ν resulting in non-dimensionalised $z^+ = zU_\tau/\nu$, and the upper abscissae is the wall normal scaled with the boundary layer thickness. In this case, we found that κ = 0.25 and B = - 1.5. The value of κ seems to deviate from the normally accepted values $0.38 < \kappa < 0.41$. The product of Kármán constant κ and and intercept B here is $\kappa B = 0.25 \times -1.5 = -0.375$, appears in the lower end of the proposed empirical relationship of κB vs. B [32]. The fluid experiences sudden favourable condition as it passes the leading edge of the airfoil [21] and it is expected that the coefficient of pressure to be within $C_p \approx -0.55$ at x/c = 47.5 % for this case. (refer Figure 3). The exposed sensor part for all measurements is l = 1.5 mm, results in non-dimensionalised sensor length $l^+ = lU_\tau/\nu \approx 25 - 35$ for all flows.

It is evident that the riblets pattern has significant effects on the boundary layer thickness δ as well as to the skin friction velocity, as shown in Table 1. It is important to discuss existing flow structure when fluid in zero pressure gradient (ZPG) is exposed to converging and diverging riblets. Converging riblets causes the local mean velocity to decrease and the turbulent intensity to increase, producing a locally thicker boundary layer [34], similar effects to exposing a flow to adverse pressure gradients (APG) [29]. In contrast, these two articles also show that diverging riblets cause the local mean velocity to increase and the turbulent intensities to decrease, producing a locally thinner boundary layer, similar to flows properties subjected to favourable pressure gradient (FPG). When converging riblets (causing APG-like environments) and measurements are taken within the adverse pressure region, we would expect the results of these conflicting conditions to be led by the dominating factor. We observe that riblets of any type cause the friction velocity, U_τ to increase. However, the converging pattern is least efficient to increase U_τ than the diverging and the directional pattern at the smooth reference point (47.5% of chord). We also we observe that the APG is the dominating parameter when mean velocity profile pattern is compared, riblets of any type cause the local mean velocities to decrease. The converging riblets cause the flow to compress, collide and force the flow to move vertically away from the wall [31]. Furthermore, the APG environments cause deceleration of the fluid especially in the wake region of the boundary layer. The converging riblets is strong enough to thicken the boundary layer, similar to the effect of APG [18] (e.g. comparison of APG-FPG). Table 1 shows that the boundary layer thickness of flow exposed to the converging δ increases by 9% when compared with the smooth surface.

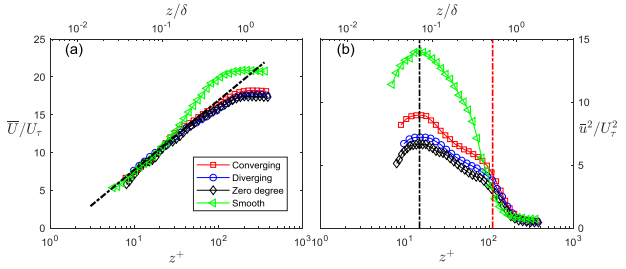


Fig. 5 : (a) Mean velocity profiles, the dashed-line indicates $1/\kappa \ln(z^+) + B$, here κ = 0.25, B = -1.5. (b) Turbulence intensities profile, dashed-dot black vertical lines indicate z^+ =15 in the near wall region and the dot-dashed red vertical lines indicate z^+ =110 in the outer region respectively.

Figure 5 (b) shows turbulence intensities profiles for flows past the smooth surface, the directional, converging or diverging riblets. The vertical axis represents the broadband turbulence intensities profile, $\bar{u}^2/U_\tau^2$. The near-wall maximum turbulence intensities for flow past a smooth surface, $\bar{u}^2/U_\tau^2|_{\max,S} \approx 14$, at z^+ = 15. It is possible that the inner peak occurs higher than the normally accepted values of $\bar{u}^2/U_\tau^2 \approx 7 - 10$ [16, 17, 18, 19, 29] due to the influences of the very large scale structures in APG. Riblets of any type, i.e. the converging, diverging and directional riblets work as a mechanism to reduce the broadband turbulence intensities and reduce the energy of the APG in the near wall

comparing to the smooth surface, where $\bar{u}^2/U_\tau^2|_{max,\ C} \approx 8.9$, $\bar{u}^2/U_\tau^2|_{max,\ D} \approx 7.2$ and $\bar{u}^2/U_\tau^2|_{max,\ Z} \approx 6.6$. The outer peak does not collapse in the outer region. Since the Reynolds number is relatively small, we use inner variables z^+ to analyze intensities in the outer region. At $z^+ = 110$, riblets of any type with yaw angle $\pm 10^o$ and aspect ratio $h/s = 0.5$ is aggressive enough to control and modify the boundary layer. Outer humps, albeit small, are observable especially for flow past converging riblets. Riblets pattern shifts inner wall energy to the outer region, evident from the formation of outer peaks where the broadband turbulence intensities $\bar{u}^2/U_\tau^2|_{max,\ C} \approx 4.5$, $\bar{u}^2/U_\tau^2|_{max,\ D} \approx 3.8$ and $\bar{u}^2/U_\tau^2|_{max,\ Z} \approx 3.2$. To understand the energy pattern due to riblet, we analyze the energy spectra.

3.3 Energy Spectra and the Large-Scale Features

In order to evaluate the effects of the riblet arrangement, the energy spectra are analyzed. All representations of pre-multiplied energy spectra $k_x\varphi_{uu}$ are plotted against streamwise wavelength $\lambda_x = 2\pi/k_x$, where wave-number $k_x = 2\pi f/U_c$, f is the frequency, and U_c is the convection velocity.

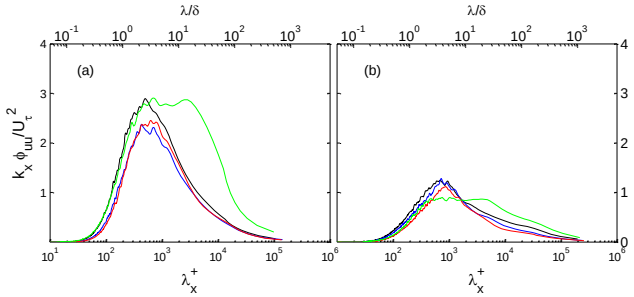


Fig. 6 : (a) z^+ =15 in the near wall region (b) 0.5δ in the outer region. Black, blue, red and green lines represent converging, diverging, zero angle riblet arrangement and the smooth surface respectively.

Figures 6(a) and 6(b) show energy spectra at $z^+ = 15$ in the near-wall region and $z = 0.5\delta$ respectively, the same locations vertical dotted-dashed line in Figure 5(b). In the near-wall region, the flow past converging riblets shows energized $\lambda_x^+ = 1000$, comparatively with higher energy as compared with the diverging and zero angle riblets as expected from the intensities plot (Figure 5(b)). Energized $\lambda_x^+ = 1000$ structures are also seen in boundary layer flows in either in ZPG, APG or FPG. The small Reynolds numbers here probably the main reason causing these features to scale with δ i.e. these streaks [22] are approximately 3-4δ structures. More interestingly, flow pasts a smooth surface displays large-scale structures that measure up to 20δ. This explains that the large near-wall peak in the intensities profile (Figure 5(b)) are significantly contributed by the large-scale structures. It suggests that the riblets break these features in the near-wall region. Similar to the typical boundary layer flow, Figure 6(b) shows energized structures approximately 4δ dominate the flow in the outer region. Again, flows past converging, diverging and zero angle riblet arrangements have similar characteristics. Flow past a smooth surface has a wide range of long structures measuring $1 < \delta < 20$. These characteristics are again not observed in boundary layer flows in ZPG, APG or FPG.

4. Conclusion

A small strip of riblets applied on a NACA 0026 airfoil causes significant effects to the flow structures. Flows on airfoil do not seem to produce profiles that follow that of internal flow as the κ and B are different from that compiled by [32]. These riblets cause the wake to reduce and follow closely to that of a favourable boundary layer profile of moderate pressure gradient (the coefficient of pressure is C_p = -0.6 in this experiment). The intensities profiles show that riblets again causes the profile to follow FPG intensities profile with converging riblets having slightly more energy as compared with the diverging and zero angle arrangements. The energy spectra analysis reveals that riblets of any type break large-scales feature measuring up to 20δ in the near-wall to break-down into smaller features. It is possible that a large-scale spanwise periodicity onto the boundary layer, resulting in a pronounced spanwise modification of the boundary layer thickness mentioned by [34], become more intense in the favourable condition. These observations probably can shed some information for researchers working on controlling vortex size and movements to control flow aerodynamics behaviours

Acknowledgement

We would like to express our gratitude for the financial support provided by UKM fundamental research grant FRGS/1/2016 /TK03/UKM/02/1 and Arus Perdana AP-2015-003.

References

[1] B. Nugroho, N. Hutchins, J. P. Monty, Effects of diverging and converging roughness on turbulent boundary layers, 18th Austr. Fluid Mech. Conf. Launceston, Australia (December), 10–13 (2012).
[2] B. Nugroho, N. Hutchins, J. P. Monty, Large-scale spanwise periodicity in a turbulent boundary layer induced by highly ordered and directional surface roughness, International Journal of Heat and Fluid Flow 41, 90–102 (2013).
[3] B. Nugroho, V. Kulandaivelu, Z. Harun, N. Hutchins, J. P. Monty, An investigation into the effects of highly directional surface roughness on turbulent boundary layers, 17th Austr. Fluid Mech. Conf. Auckland, New Zealand (December), 6-9 (2010).
[4] D. Goldstein, R. Handler, L. Sirovich, Direct numerical simulation of turbulent flow over a modeled riblet covered surface, Journal of Fluid Mechanics 302, 333 (1995).
[5] D. W. Bechert, M. Bruse, W. Hage, Experiments with three-dimensional riblets as an idealized model of shark skin, Experiments in Fluids 28 (5), 403–412 (2000).
[6] D. W. Bechert, M. Bruse, W. Hage, J. G. T. Van Der Hoeven, G. Hoppe, Experiments on drag-reducing surfaces and their optimization with an adjustable geometry, Journal of Fluid Mechanics 338, 59–87 (1997).
[7] F. E. Fish, L. E. Howle, M. M. Murray, Hydrodynamic flow control in marine mammals, Integrative and Comparative Biology 48 (6), 788–800 (2008).
[8] F. Muhsin, W. F. M. Yusoff, M. F. Mohamed, A. R. Sapian, CFD modeling of natural ventilation in a void connected to the living units of multi-storey housing for thermal comfort, Energy and Buildings 144, 1–16 (2017).
[9] H. Chen, F. Rao, X. Shang, D. Zhang, I. Hagiwara, Biomimetic drag reduction study on herringbone riblets of bird feather, Journal of Bionic Engineering 10 (3), 341–349 (2013).
[10] H. Chen, F. Rao, X. Shang, D. Zhang, I. Hagiwara, Flow over bio-inspired 3D herringbone wall riblets, Experiments in Fluids 55 (3-1698), 1–7 (2014).
[11] H. M. Nagib, K. A. Chauhan, Variations of von Kármán coefficient in canonical flows, Physics of Fluids 20 (10), 1–11 (2008).
[12] Howard W. Emmon, Flow of a compressible fluid past a symmetrical airfoil in a wind tunnel and in free air, Journal of the Physical Society of Japan 25, 1703–1722 (1948).
[13] J. P. Monty, Z. Harun, I. Marusic, A parametric study of adverse pressure gradient turbulent boundary layers, International Journal of Heat and Fluid Flow 32 (3), 575–585 (2011).
[14] J. Yunus, A.C. and Cimbala, Fluid Mechanics Fundamentals and Applications, 3rd Edition, McGraw Hill Publication, 185201, (2006).
[15] K.-S. Choi, Near-wall structure of a turbulent boundary layer with riblets, Journal of Fluid Mechanics 208, 417–458 (1989).
[16] M. I. Ghazali, Z. Harun, W. A. W. Ghopa, A. A. Abbas, Computational Fluid Dynamic Simulation on NACA 0026 airfoil with v-groove riblets, International Journal on Advanced Science, Engineering and Information Technology 6 (4), 529-533 (2016).
[17] M. J. Walsh, Riblets as a viscous drag reduction technique, AIAA Journal 21 (4), 485–486 (1983).

[18] N. Hutchins, I. Marusic, Evidence of very long meandering features in the logarithmic region of turbulent boundary layers, Journal of Fluid Mechanics 579, 1–28 (2007).
[19] N. Hutchins, T. B. Nickels, I. Marusic, M. S. Chong, Hot-wire spatial resolution issues in wall-bounded turbulence, Journal of Fluid Mechanics 635, 103–136 (2009).
[20] N. Lin, W.P., White, B.R. and Bagheri, Experiments on the Large-Scale Structure of Turbulent Boundary Layers with Adverse Pressure Gradients, In 33rd Aerospace Sciences Meeting and Exhibit 21 (1995).
[21] P. Luchini, F. Manzo, A. Pozzi, Resistance of a grooved surface to parallel flow and cross-flow, Journal of Fluid Mechanics 228, 87–109 (1991).
[22] P. M. Ligrani, P. Bradshaw, Spatial resolution and measurement of turbulence in the viscous sublayer using subminiature hot-wire probes, Experiments in Fluids 5 (6), 407–417 (1987).
[23] R. Garcia-Mayoral, J. Jimenez, Drag reduction by riblets, Philosophical Transactions of the Royal Society A: Mathematical, Physical and Engineering Sciences 369, 1412–1427 (2011).
[24] R. Koeltzsch, K ., Dinkelacker, A., Grundmann, Flow over convergent and divergent wall riblets, Experiments in Fluids 33 (2) (2002) 346–350.
[25] S. M. A. Aftab, N. A. Razak, A. S. Mohd Rafie, K. A. Ahmad, Mimicking the humpback whale: An aerodynamic perspective, Progress in Aerospace Sciences 84, 48–69 (2016).
[26] S. P. Wilkinson, Viscous drag reduction in boundary layers, Vol. 1, AIAA Journal, (1990).
[27] T. Nadesan, H. Mitsudharmadi, T. S. Lee, S. H. Winoto, Quasi-streamwise counter-rotating vortices generated by convergent riblets in flat plate boundary layer, Journal of Visualization 17, 319–325 (2014).
[28] W. Hage, D. W. Bechert, M. Bruse, Yaw angle effects on optimized riblets, Aerodynamic Drag Reduction Technologies 278–285 (2001).
[29] Y. Luo, L. Wang, L. Green, K. Song, L. Wang, R. Smith, Advances of drag-reducing surface technologies in turbulence based on boundary layer control, Journal of Hydrodynamics 27 (4), 473-487 (2015).
[30] Y. Luo, L. Yuan, J. Li, J. Wang, Boundary layer drag reduction research hypotheses derived from bio-inspired surface and recent advanced applications, Micron 79, 59–73 (2015).
[31] Z. Harun, A. A. Abbas, A. Etminan, B. Nugroho, V. Kulandaivelu, M. Khashehchi, Effects of riblet on flow structure around a NACA 0026 airfoil, The 25th International Symposium on Transport Phenomena, Krabi, Thailand (November), 1–7 (2014).
[32] Z. Harun, A. A. Abbas, R. M. Dheyaa, M. I. Ghazali, Ordered roughness effects on NACA 0026 airfoil, IOP Conference Series: Materials Science and Engineering 152 (1), 012005 (2016).
[33] Z. Harun, I. Marusic, J. P. Monty, R. Mathis, Effects of pressure gradient on higher order statistics in turbulent boundary layers, Turbulence, Heat and Mass Transfer 7, 1–12 (2012).
[34] Z. Harun, J. P. Monty, I. Marusic, The structure of zero, favorable and adverse pressure gradient turbulent boundary layers, 7th International Symposium on Turbulence and Shear Flow Phenomena, Ottawa, Canada 1–6 (2010).
[35] Z. Harun, J. P. Monty, R. Mathis, I. Marusic, Pressure gradient effects on the large-scale structure of turbulent boundary layers, Journal of Fluid Mechanics 715, 477–498 (2013).
[36] Z. Harun, M. Isa, M. Rasani, S. Abdullah, The effects of spatial resolution in turbulent boundary layers with pressure gradients, Applied Mechanics and Materials 225, 109–117 (2012).
[37] Z. Harun, V. Kulandaivelu, B. Nugroho, M. Khashehchi, J. P. Monty, I. Marusic, Large scale structures in an adverse pressure gradient turbulent boundary layer, 12th International Symposium on Engineering Turbulence Modelling and Measurements (ETMM12), Marseilles (June 2010).
[38] Z. Harun, W. A. W. Ghopa, A. Abdullah, M. I. Ghazali, A. A. Abbas, M. R. Rasani, R. Zulkifli, W. M. F. Wan Mahmood, M. R. Abu Mansor, Z. Zainol Abidin, W. H. M. Wan Mohtar, The development of a multipurpose wind tunnel, Jurnal Teknologi 10, 63–70 (2016).